Scientific Research Publishing

Materials Sciences and Applications, 2026, 17(3), 75-88
https://www.scirp.org/journal/msa
ISSN Online: 2153-1188
ISSN Print: 2153-117X

Influence of Microstructure on the Passivation and Corrosion Behaviour of a High Carbon Steel

Francesco Rosalbino

Dipartimento di Scienza dei Materiali e Ingegneria Chimica (DICHI), Politecnico di Torino, Torino, Italy
Email: francesco.rosalbino@polito.it

How to cite this paper: Rosalbino, F. (2026) Influence of Microstructure on the Passivation and Corrosion Behaviour of a High Carbon Steel. *Materials Sciences and Applications*, **17**, 75-88.
https://doi.org/10.4236/msa.2026.173006

Received: January 29, 2026
Accepted: March 20, 2026
Published: March 23, 2026

Abstract

The effect of bainite and tempered martensite on the passivation and corrosion behaviour of a steel with composition 0.70C, 0.22Si, 0.60Mn, 0.017P, 0.012S (wt%) is investigated in aerated borate buffer solution, pH = 9.2, and with addition of 100 mM KCl. In the absence of chloride ions, free corrosion potential measurements and impedance spectroscopy tests have shown lower barrier properties of passive film grown on tempered martensitic microstructure as compared to the one formed on bainitic microstructure. Moreover, the electrochemical measurements highlight superior corrosion resistance displayed by the bainitic steel in the presence of chloride ions with respect to the tempered martensitic steel. The observed behaviour is ascribed to the shape, size, and distribution of the ferrite and cementite.

Keywords

Carbon Steel, Bainite, Tempered Martensite, Passive Film, Electrochemical Impedance Spectroscopy (EIS)

1. Introduction

Corrosion of steel is a major problem in the petroleum, chemical, automotive and construction industries. Corrosion of steel depends on several factors, such as environment, material composition, and microstructure. These factors are also crucial in deciding the life of the components [1]. Microstructure and composition play a very important role in deciding the corrosion susceptibility of steel, as reported by several researchers [2]-[8].

A wide range of industries such as aerospace, automotive, oil and gas employ high-strength steels due to their mechanical properties in efforts to reduce weight in structures and save energy in transportation applications. The exceptional mechanical properties of these steels (an advantageous combination of strength, duc-

tility and plasticity) often result from a particular microstructure created through a precise balance between kinetic processes and thermodynamics [9]. Martensitic and bainitic transformations have been used in the development of high-strength and/or high-ductility steels [10]-[13]. Improving the properties of steel by controlling these transformations requires an in-depth understanding of the relationship between the properties and microstructures.

Clover *et al.* [14] showed that tempered martensite has a higher corrosion rate than the ferrite/pearlite microstructure in the stirred autoclave operating with a CO_2 environment. Kazum *et al.* [7] reported a higher corrosion rate for a martensitic steel than that of a nanostructured bainitic steel in 3.5% NaCl. The nanostructured bainitic steel shows only general corrosion, whereas the martensitic steel reveals a high rate of localized corrosion. Moon *et al.* [4] showed that, in 3.5% NaCl solution, conventional C-Mn pearlitic steel exhibits lower corrosion current density than does bainitic steel.

The steel with 0.7 wt% carbon is predominantly used in making rail, spring and cutting tools. The electrochemical properties of high carbon steel depend heavily on the morphology of cementite (Fe_3C) in the ferrite matrix [8]. On the other hand, for the same composition of steel, the microstructure and, subsequently, size and distribution of different phases can be altered by various heat treatment practices, such as normalizing, isothermal transformation, oil quenching and tempering [14]-[16]. Hence, it would be interesting to see the effect of different microstructures made from a single composition of steel on the electrochemical behaviour.

Despite recognizing the importance of the morphology of microstructure on the corrosion susceptibility of steel [2]-[8] [13] [17]-[19], not much work is reported in the literature where, for a given composition of steel the influence of constituent microstructures, namely, bainite and tempered martensite, was researched.

In the present study, specimens composed of bainite and tempered martensite were prepared using Fe-0.70C-0.22Si-0.60Mn steel. The corrosion behaviour of each microstructure was assessed with the help of open circuit potential and electrochemical impedance spectroscopy techniques in borate buffer solution, pH = 9.2, and in borate buffer solution containing KCl.

2. Experimental Details

The chemical composition of the high carbon steel used in the present work is reported in Table 1. The sheet was cut into approximately 15 × 12 × 1.5 mm coupons.

Table 1. Chemical composition of the investigated steel in wt%.

C	Si	Mn	P	S
0.70	0.22	0.60	0.017	0.012

To obtain specimens with bainitic microstructure, one set of coupons was austenitized at 950˚C for 0.5 h in a tube furnace, followed by isothermal transformation (0.5 h) at 300˚C using a high temperature salt bath of composition $BaCl_2$ + 25% KCl + 20% NaCl followed by water quenching. Another set of coupons was austenitized at 950˚C for 0.5 h, followed by oil quenching. The oil quenched samples were heated in a muffle furnace at 400˚C for 0.5 h to obtain a tempered martensite microstructure.

For the microstructure analysis and hardness measurement, the steel specimens were ground on silicon carbide papers up to 1200 grit size followed by cloth polishing with suspension alumina powder of size up to 0.05 μm. The hardness measurements of the steel samples were performed in a Tinius Olsen digital machine. All the Rockwell hardness (HRC) tests of the selected steel specimens were carried out with the help of a spheroconical diamond indenter at a load of 150 kg.

The etching of the polished samples was done using 3% Nital solution to reveal the microstructures. Microstructural observations were carried out using a Leica Microsystem optical microscope and field emission-scanning electron microscope (Nova Nano FE-SEM 450).

For electrochemical measurements, all the samples were abraded with 1200 grit SiC emery paper followed by diamond paste (down to 0.05 μm), then degreased in isopropyl alcohol in an ultrasonic bath, dried in air and stored in a desiccator. Specimens were electrochemically studied in a three-electrode cell at 25˚C ± 1˚C using a saturated calomel electrode (SCE) as reference electrode and a platinum wire as counter electrode. The electrochemical experiments were carried out in 0.075 M $Na_2B_4O_7$ + 0.5 M H_3BO_3 (pH = 9.2) and with the addition of 100 mM KCl. All reagents, in analytical grade, were provided by Sigma-Aldrich. The electrolytic medium was naturally aerated and the experiments were conducted without stirring.

Open circuit potential, E_{OC}, was measured with respect to the SCE every 60 s for a period of 2 h.

Electrochemical impedance spectroscopy (EIS) measurements were carried out at open circuit potential using an EG & G PAR system Model 2263 driven by a computer. The impedance spectra were acquired in the frequency range from 100 kHz to 10 mHz with a perturbation signal of 10 mV at seven points per decade. EIS plots were obtained after 2 h exposure to the test solution. Experimental data were stored in the computer and processed according to the EQUIVCRT program (B. A. Boukamp, University of Twente).

3. Results and Discussion

The optical micrographs of the steel samples after Nital etching are reported in Figure 1. Figure 1(a) shows the bainitic microstructure, which is a mixture of ferrite and cementite, but in non-lamellar form. The tempered martensite microstructure is displayed in Figure 1(b), where carbide particles are located at the plate boundaries of the needle-shaped ferrite morphology.

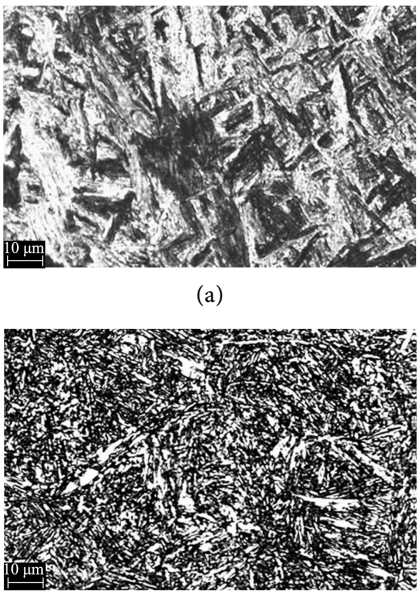

(a)

(b)

Figure 1. Optical micrographs of the: (a) bainitic steel and (b) tempered martensitic steel (needles) after Nital etching.

FE-SEM micrographs obtained from the preceding specimens are reported in **Figure 2**. White colored cementite (Fe_3C) phase with a different morphology and grey colored ferrite phase are clearly observed in these micrographs. The bainitic structure is shown in **Figure 2(a)** with a featherlike morphology. The tempered martensite morphology is displayed in **Figure 2(b)**.

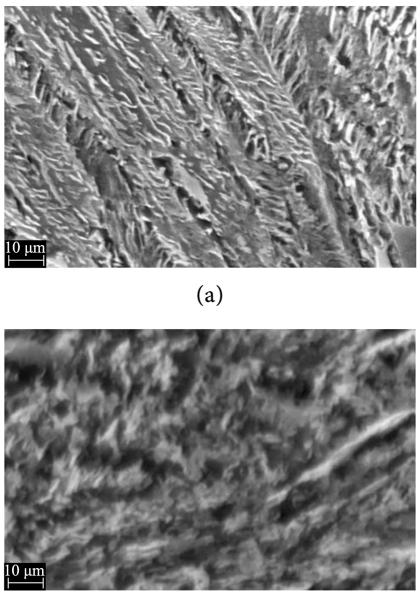

(a)

(b)

Figure 2. Fe-SEM micrographs of the: (a) bainitic steel and (b) tempered martensitic steel after Nital etching. The white color in the micrographs represents the cementite phase with different morphologies, and the gray color shows the ferrite phase.

The hardness values of the steel specimens are listed in Table 2. As can be seen, bainitc steel has a higher hardness value than tempered martensitic steel. The hardness values ensure the uniformity of the developed microstructures of the steel specimens after two different heat treatment processes. The obtained hardness results match with the published literature on similar microstructures [15] [20].

Table 2. Rockwell C hardness of the steel specimens.

Specimen	Hardness (HRC)
Bainitic steel	52.05 ± 0.44
Tempered martensitic steel	45.22 ± 0.19

The open circuit potential, E_{OC}, of bainitic and tempered martensitic steels in borate buffer solution was monitored for a period of 2 h. As can be seen in Figure 3, the open circuit transients measured for both steels have similar trend, where E_{OC} from the instant of exposure shifts with time in the positive direction, indicating a spontaneous passivation due to development of an oxide film [21]. This continues as a result of the predominance of the cathodic processes over the anodic ones until the film acquires a stable thickness. The necessary electrons of the cathodic reaction are provided by the ionization of metal atoms (Fe atoms) entering the oxide phase. For the bainitic steel the initial open circuit potential is −350 mV (SCE), then it gradually changes towards more positive values and after 2 h of exposure a potential of −290 mV (SCE) is reached. The time profiles of E_{OC} obtained for the tempered martensitic steel is similar. The initial E_{OC} is −415 mV (SCE), then it progressively increases to nobler potentials reaching after 2 h a steady value of about −350 mV (SCE).

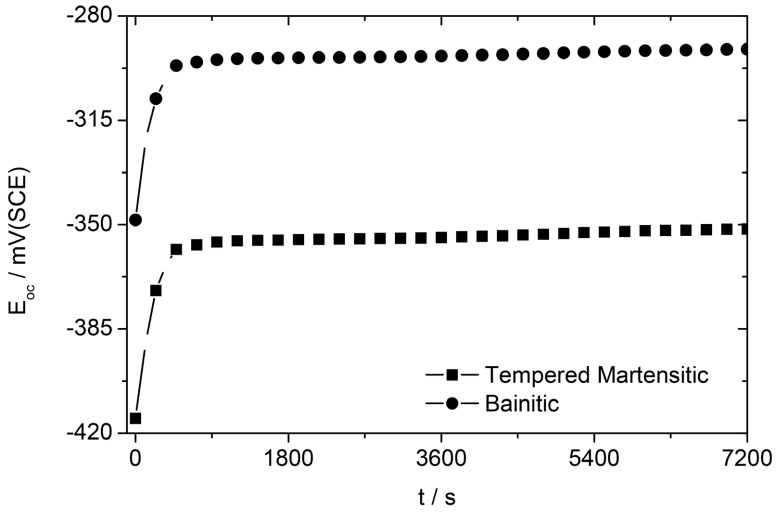

Figure 3. Open circuit potential vs. time profile of the steel specimens after 2 h exposure to 0.075 M $Na_2B_4O_7$ + 0.05 H_3BO_3 solution (pH = 9.2).

The initial E_{OC} increase observed for both the investigated steels can be ascribed to the thickening of the passive film formed at the specimen surface, thereby improving its protection ability in borate buffer solution [22]. The open circuit potential increases until the oxide layer reaches its limiting protective capacity, thus resulting in stabilization of E_{OC} [23] [24]. As can be seen in **Figure 1**, the tempered martensitic specimen exhibits lower E_{OC} values with respect to the bainitic sample, suggesting inferior barrier capabilities for the passive film formed at its surface.

Figure 4 reports the EIS spectra, in the form of Nyquist diagrams, of bainitic and tempered martensitic steels at open circuit potential, after 2 h exposure to borate buffer solution. Both Nyquist diagrams present a single depressed and incomplete capacitive semicircle, however the bainitic specimen exhibits a higher impedance value as compared with the tempered martensitic sample, thereby confirming the better barrier properties of its surface oxide layer in agreement with the results obtained from open circuit potential measurements.

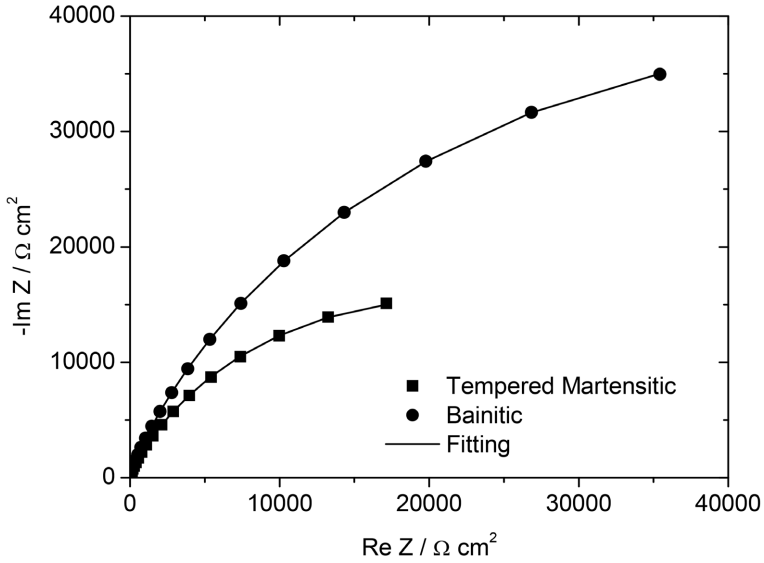

Figure 4. Experimental and simulated Nyquist diagrams for the steel specimens after 2 h exposure 0.075 M $Na_2B_4O_7$ + 0.05 H_3BO_3 solution (pH = 9.2).

The impedance spectra obtained have been interpreted in terms of an equivalent circuit, with the circuit elements representing electrochemical properties of the alloy and its surface passive film. Both the steel specimens characterized by EIS at their open circuit potential can be described by an equivalent circuit model with one time constant, and good agreement between experimental data and fitted data is obtained. The proposed equivalent circuit, shown in **Figure 5**, assumes the presence of a surface oxide film that acts as a barrier-type single compact layer [25] [26]. The equivalent circuit consists of a series combination of the electrolytic solution resistance, R_s, and a single parallel constant phase element/resistor pair, Q_{ox}/R_{ox}, describing the properties of the passive film formed on the investigate materials, respectively the capacitance and resistance of the oxide layer.

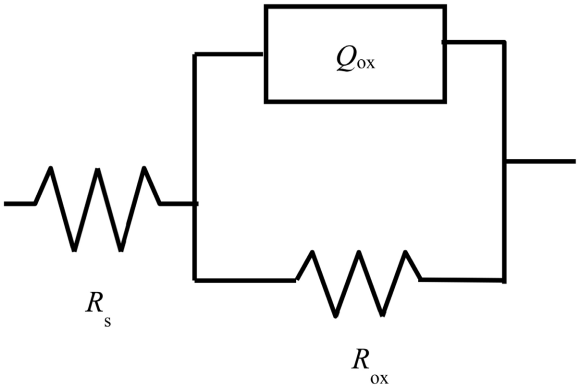

Figure 5. Proposed equivalent circuit for modeling experimental impedance data.

A constant phase element, CPE, was used for fitting the impedance spectra instead of a pure capacitance owing to the non-ideal capacitive response due to the distributed relaxation feature of the oxide film, which is observed as a depressed semicircle in the Nyquist diagrams. The impedance of the CPE is given by:

$$Z_{\mathrm{CPE}} = \left[Y_0 \left(j\omega \right)^n \right]^{-1} \tag{1}$$

where Y_0 is a constant, $j^2 = -1$ is the imaginary number, ω is the angular frequency and $-1 \le n \le 1$. The value of n seems to be associated with the non-uniform distribution of current as a result of roughness and surface defects [27].

Analysis of the EIS spectra in terms of the equivalent circuit shown in **Figure 4** allows the parameter Q_{ox} and R_{ox} to be determined, and their values are reported in **Table 3**. The agreement between experimental and simulated data indicates that the experimental impedance spectra are well fitted to the proposed equivalent circuit. The fitting quality was evaluated by chi-squared (χ^2) values of about 10^{-4}, with a relative error less than 5%. On the Nyquist plots in **Figure 3**, the experimental data are shown as individual points, while the fitted spectra are presented as continuous lines.

Table 3. Electrical parameters of the equivalent circuit for bainitic and tempered martensitic steels in borate buffer solution, pH = 9.2, at 25˚C.

Specimen	Q_{ox} (10^5 S·cm^{-2}·s^n)	n	R_{ox} (Ω·cm^2)	C_{ox} (F·cm^{-2})	d (nm)
Bainitic	1.9	0.91	1.62×10^4	2.06×10^{-5}	2.23
Tempered martensitic	2.5	0.89	9.51×10^3	3.78×10^{-5}	1.14

Capacitance values of the passive oxide film can be extracted from the CPE parameter, Q_{ox}, using [28]:

$$C_{ox} = \left(R_{ox}^{1-n} Q_{ox} \right)^{1/n} \tag{2}$$

and are given in **Table 3**.

Comparing the capacitances for bainitic and tempered martensitic steels, it is

possible to observe that the tempered martensitic specimen has a higher capacitance value (about 38 μF·cm^{-2}) with respect to the bainitic sample. This indicates a better capacitive effect of the oxide layer formed on the bainitic steel, thereby confirming the previous E_{OC} measurements.

By considering the oxide film to act as a parallel plate dielectric, the passive layer thickness can be calculated according to [29]:

$$C = \varepsilon\varepsilon_0 A d^{-1} \tag{3}$$

where ε is the dielectric constant of the oxide, ε_0 the vacuum permittivity, A the geometric area and d is the thickness. From the capacitance, C_{ox}, values extracted from the CPE parameter, Q_{ox}, the thickness of the oxide film formed on the studied steels can be estimated. To that end, $\varepsilon = 12.0$ is assumed, which is the value for the oxide layer formed on carbon steels [30]. The thickness of the passive film grown on the investigated materials during exposure to borate buffer solution is reported in **Table 3**. As can be seen, the oxide layer on bainitic steel shows higher values of resistance and thickness than the tempered martensitic steel, which indicates a more compact passive film with better barrier properties. The observed behaviour can be ascribed to the particular microstructure morphology of tempered martensitic specimen that would lead to the formation of a more defective oxide layer [31] [32].

Figure 6 shows the evolution of the open-circuit potential, E_{OC}, of bainitic and tempered martensitic steels as a function of exposure time in borate buffer + 100 mM KCl solution. As can be seen, the E_{OC} drops in the negative direction and tend to stabilizes for long exposure times. This indicates breakdown of the protective oxide film and subsequent surface activation. The E_{OC} curve of bainitic steel exhibits a negative shift at a steady state potential of approximately −425 mV (SCE) while tempered martensitic steel has a negative shift with a steady state potential of −480 mV (SCE). The higher E_{OC} of banitic specimen is indicative of its nobler character with respect to tempered martensitic sample.

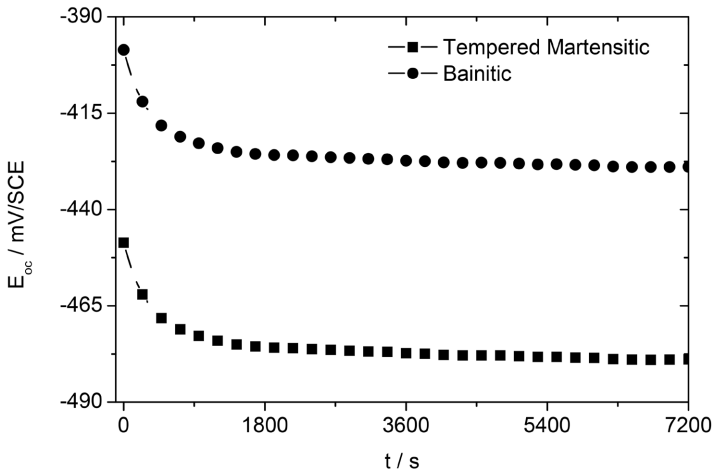

Figure 6. Open circuit potential vs. time profile of the steel specimens after 2 h exposure to borate buffer + 100 mM KCl solution.

Figure 7 reports the EIS spectra, in the form of Nyquist diagrams, of bainitic and tempered martensitic steels at open circuit potential, after 2 h exposure to borate buffer + 100 mM KCl solution. The impedance spectra are characterized by a depressed semicircle with a capacitive arc. Compared with tempered martensitic specimen, the bainitic sample exhibits a higher impedance value, indicating better corrosion behaviour in the presence of chloride ions.

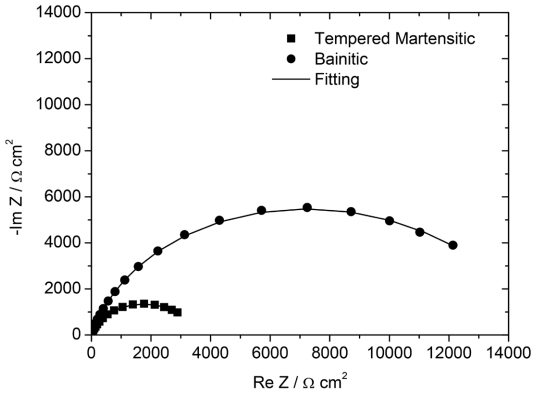

Figure 7. Experimental and simulated Nyquist diagrams for the steel specimens after 2 h exposure to borate buffer + 100 mM KCl solution.

Based on the impedance responses of the investigated alloys, an appropriate equivalent circuit was proposed as shown in Figure 8. Experimental EIS data were best fitted using proposed equivalent circuit. The accuracy of fitting results, shown as solid lines in Figure 6, was evaluated by the chi-squared (χ^2) values, which were in the order of 10^{-4} for both specimens. The equivalent circuit includes the solution resistance, R_s, in series with one RC (time constant), $\tau = R{\cdot}\text{CPE}$, representing the faradaic charge transfer process. The elements R_{ct} and Q_{dl} can be attributed to the metal/electrolyte interface in which R_{ct} is the charge transfer resistance related to the rate of corrosion reactions at the open circuit potential, and Q_{dl} represents the double layer capacitance [33] [34]. A constant phase element (CPE), defined as Q, is introduced in the equivalent circuit instead of a pure capacitance. The values of fitted parameters are reported in Table 4. As can be seen, the charge transfer resistance of bainitic specimen exhibits a fourfold higher value than the tempered martensitic sample, indicating better corrosion behaviour. Since the corrosion rate is inversely related to R_{ct}—the higher the value of R_{ct} the higher the corrosion resistance (lesser corrosion rate) [35] [36], the larger R_{ct} value showed by the bainitic specimen with respect to the tempered martensitic sample highlights its higher stability in the presence of chloride ions.

Table 4. Electrical parameters of the equivalent circuit for bainitic and tempered martensitic steels in borate buffer + 100 mM KCl at 25˚C.

Specimen	Q_{dl} (10^5 S·cm^{-2}·s^{-n})	n_{dl}	R_{ct} (Ω·cm^2)
Bainitic	2.8	0.89	13.51×10^3
Tempered martensitic	3.5	0.87	3.34×10^3

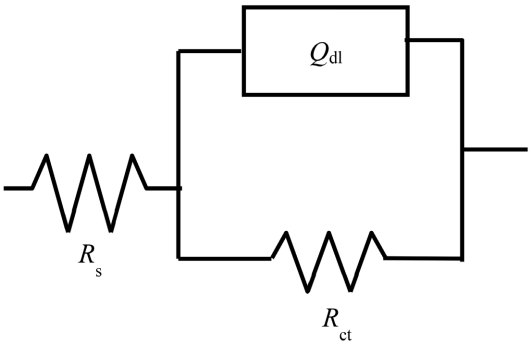

Figure 8. Equivalent electrical circuit used for EIS modeling.

Figure 9 reports the SEM-FE micrographs of the surface of bainitic and tempered martensitic steels after 2 h exposure to borate buffer + 0.1 M KCl solution. These micrographs are not taken after etching, suggesting that the dissolution of the ferritic region in the ferrite-cementite microgalvanic couple enables the microstructure to become resolved. The corrosion morphology of bainitic steel, **Figure 9(a)**, reveals the presence of white fine flaky particles with thickness less than 20 nm covering almost homogeneously the surface. Flaky white regions are also seen in the etched sample of the bainitic steel (**Figure 2(a)**). However, after 2 h exposure to chloride ions, these flaky particles have evolved clearly. The protruded nature of these particles also confirms that cementite acts as a cathode in the microgalvanic cell formed between the overall ferritic portion and cementite flaky particles.

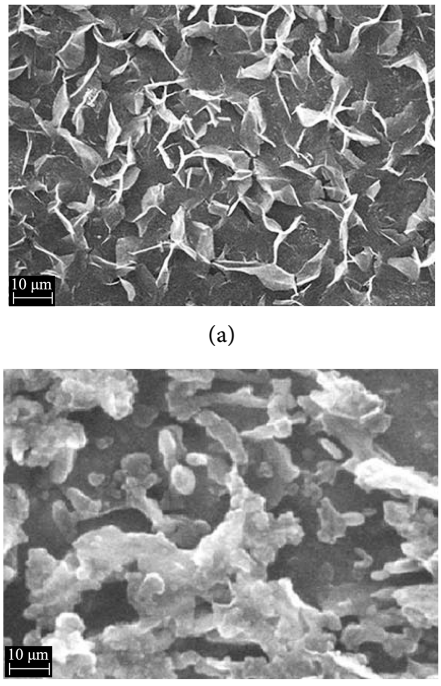

(a)

(b)

Figure 9. Fe-SEM micrographs of the: (a) bainitic steel and (b) tempered martensitic steel after 2 h exposure to borate buffer + 100 mM KCl solution.

On the other hand, the corrosion morphology of the tempered martensitic steel after 2 h exposure to chloride ions is shown in Figure 9(b). A significant corrosion attack is visible since the cementite particles are interconnected (white network), and this allows a very large cathodic area leading to higher ferrite dissolution.

The basic mechanism for corrosion in bainitic and tempered martensitic steels is similar, where cementite and ferrite are a cathode and anode, respectively, in the galvanic couple. However, the size, shape, and distribution of constituents in the microstructures lead to a change in the length scales of the galvanic couples. In both alloys, a distributed galvanic couple exists due to the non-lamellar shape of cementite. In bainitic steel (Figure 9(a)), the dissolution mode is on a very fine length scale (≈100 to 200 nm) since the carbides are very thin here. By contrast, in the case of tempered martensitic steel (Figure 9(b)), there is a network of cementite that actually leads to the formation of interconnected cathodes, enabling the surrounding ferrite to dissolve more quickly as a result of the high interfacial contact area between the two phases.

The present results corroborate with some of the literature reports. Kazum *et al.* reported better corrosion resistance of the bainitic steel as compared to the tempered martensitic steel, and the same was observed in the present study [7]. However, the steel compositions, as mentioned in the work of Kazum *et al.*, are different. The present study clearly brought out the effects of the morphologies of bainite and tempered martensite on their electrochemical responses, since both steels are made from the same composition. Hence, it is clear that the present study analyzes both the microstructures and compares their corrosion properties convincingly, since they are made from a single composition.

The novelty in the present work is the effect of two microstructures on the corrosion behavior of steel *via* electrochemical techniques and both the microstructures being generated from a single composition. It is well understood that composition and microstructures both have a strong influence on the corrosion behavior of metals and alloys, specifically of steel. Now, the present work avoided complications from different compositions of the steels and studied only the effect of microstructures on the corrosion behavior of steel. One can also see the influence of cementite and ferrite phases having various morphologies for steels with different compositions. However, in that case, it is not possible, with certainty, to understand the separate effects of microstructures and composition on the corrosion behavior of steel.

4. Conclusions

In this paper, the role of microstructure on the passivation and corrosion behaviour of a high carbon steel low alloy steels is investigated in borate buffer solution and with addition of 100 mM KCl. The effect of bainite and tempered martensite phases is analysed by means of free corrosion potential and electrochemical impedance spectroscopy measurements.

In the absence of chloride ions, tempered martensitic steel exhibits lower bar-

rier properties of its passive film with respect to bainitic steel, as a consequence of the particular microstructure morphology that would lead to the formation of a more defective oxide layer.

In the presence of chloride ions, the bainitic specimen displays higher corrosion resistance as compared to the tempered martensitic sample. Though the corrosion starts and continues with the creation of galvanic cell between cathodic carbide and anodic ferrite phases, corrosion mechanism differs for both the steels with different microstructure, attributing to the size, shape, and distribution of galvanic couple.

Conflicts of Interest

The author declares no conflicts of interest regarding the publication of this paper.

References

[1] Fontana, M.G. (1987) Corrosion Engineering. McGraw-Hill.

[2] López, D.A., Schreiner, W.H., de Sánchez, S.R. and Simison, S.N. (2003) The Influence of Carbon Steel Microstructure on Corrosion Layers: An XPS and SEM Characterization. *Applied Surface Science*, **207**, 69-85. https://doi.org/10.1016/s0169-4332(02)01218-7

[3] Balasubramaniam, R., Panda, B., Dwivedi, G., Moon, A.P. and Mahapatra, S. (2011) Alloy Development of Corrosion-Resistant Rail Steel. *Current Science*, **100**, 52-57.

[4] Moon, A.P., Sangal, S., Layek, S., Giribaskar, S. and Mondal, K. (2015) Corrosion Behavior of High-Strength Bainitic Rail Steels. *Metallurgical and Materials Transactions A*, **46**, 1500-1518. https://doi.org/10.1007/s11661-014-2732-0

[5] Souza, E.C.D., Rossitti, S.M., Fortulan, C.A. and Rollo, J.M.D.D.A. (2016) Influence of Ferrite Phase Content on the Electrochemical Properties of Duplex Stainless Steels. *Materials Research*, **20**, 21-29. https://doi.org/10.1590/1980-5373-mr-2016-0546

[6] López, D.A., Simison, S.N. and de Sánchez, S.R. (2003) The Influence of Steel Microstructure on CO_2 Corrosion. EIS Studies on the Inhibition Efficiency of Benzimidazole. *Electrochimica Acta*, **48**, 845-854. https://doi.org/10.1016/s0013-4686(02)00776-4

[7] Kazum, O., Bobby Kannan, M., Beladi, H., Timokhina, I.B., Hodgson, P.D. and Khoddam, S. (2014) Aqueous Corrosion Performance of Nanostructured Bainitic Steel. *Materials & Design* (1980-2015), **54**, 67-71. https://doi.org/10.1016/j.matdes.2013.08.015

[8] Cleary, H.J. and Greene, N.D. (1967) Corrosion Properties of Iron and Steel. *Corrosion Science*, **7**, 821-831. https://doi.org/10.1016/s0010-938x(67)80115-x

[9] Sietsma, J. (2013) Physical Modelling the Microstructure Formation in Advanced High-Strength Steels. *Materials Science Forum*, **762**, 194-209. https://doi.org/10.4028/www.scientific.net/msf.762.194

[10] Zhang, X., Miyamoto, G., Toji, Y., Zhang, Y. and Furuhara, T. (2021) Role of Cementite and Retained Austenite on Austenite Reversion from Martensite and Bainite in Fe-2Mn-1.5Si-0.3C Alloy. *Acta Materialia*, **209**, Article ID: 116772. https://doi.org/10.1016/j.actamat.2021.116772

[11] Sakaguchi, N., Ohno, H. and Nakada, N. (2022) Simultaneous Optimization of Rigidity and Strength of Super Invar Cast Steel Using by Martensitic Reversion. *ISIJ Inter-*

national, **62**, 586-592. https://doi.org/10.2355/isijinternational.isijint-2021-478

[12] Ogawa, T., Maruyama, N., Sugiura, N. and Yoshinaga, N. (2010) Incomplete Recrystallization and Subsequent Microstructural Evolution during Intercritical Annealing in Cold-Rolled Low Carbon Steels. *ISIJ International*, **50**, 469-475. https://doi.org/10.2355/isijinternational.50.469

[13] Takagi, S., Toji, Y., Yoshino, M. and Hasegawa, K. (2012) Hydrogen Embrittlement Resistance Evaluation of Ultra High Strength Steel Sheets for Automobiles. *ISIJ International*, **52**, 316-322. https://doi.org/10.2355/isijinternational.52.316

[14] Clover, D., Kinsella, B., Pejcic, B. and De Marco, R. (2005) The Influence of Microstructure on the Corrosion Rate of Various Carbon Steels. *Journal of Applied Electrochemistry*, **35**, 139-149. https://doi.org/10.1007/s10800-004-6207-7

[15] Callister, W. and Rethwisch, D. (2007) Materials Science and Engineering: An Introduction. Wiley.

[16] Zhang, X.Z. and Knot, J.F. (1999) Clevage Fracture in Bainitic and Martensitic Microstructures. *Acta Materialia*, **47**, 3483-3495. https://doi.org/10.1016/S1359-6454(99)00200-1

[17] Rault, V., Vignal, V., Krawiec, H. and Tadjoa, O. (2014) Corrosion Behaviour of Heavily Deformed Pearlitic and Brass-Coated Pearlitic Steels in Sodium Chloride Solutions. *Corrosion Science*, **86**, 275-284. https://doi.org/10.1016/j.corsci.2014.06.002

[18] Oluyemi, D.O., Oluwole, O.I. and Adewuyi, B.O. (2011) Studies of the Properties of Heat Treated Rolled Medium Carbon Steel. *Materials Research*, **14**, 135-141. https://doi.org/10.1590/s1516-14392011005000040

[19] Al-Rubaiey, S.I., Anoon, E.A. and Hanoon, M.M. (2013) The Influence of Microstructure on the Corrosion Rate of Carbon Steels. *Engineering and Technology Journal*, **31**, 1825-1836. https://doi.org/10.30684/etj.31.10a2

[20] Arai, T. (2001) Heat Treating, ASM Handbook. ASM International.

[21] Shams El Din, A.M. and Paul, N.J. (1990) Oxide Film Thickening on the Surface of Metals in Aqueous Solutions: A Critique of the Theory of Open-Circuit Potential Transients. *Thin Solid Films*, **189**, 205-216. https://doi.org/10.1016/0040-6090(90)90449-n

[22] Lavos-Valereto, I.C., Costa, I. and Wolynec, S. (2002) The Electrochemical Behavior of Ti-6Al-7Nb Alloy with and without Plasma-Sprayed Hydroxyapatite Coating in Hank's Solution. *Journal of Biomedical Materials Research*, **63**, 664-670. https://doi.org/10.1002/jbm.10351

[23] Patrito, E.M., Torresi, R.M., Leiva, E.P.M. and Macagno, V.A. (1990) Potentiodynamic and AC Impedance Investigation of Anodic Zirconium Oxide Films. *Journal of The Electrochemical Society*, **137**, 524-530. https://doi.org/10.1149/1.2086492

[24] Pauporté, T., Finne, J., Kahn-Harari, A. and Lincot, D. (2005) Growth by Plasma Electrolysis of Zirconium Oxide Films in the Micrometer Range. *Surface and Coatings Technology*, **199**, 213-219. https://doi.org/10.1016/j.surfcoat.2005.03.003

[25] Khalil, N., Bowen, A. and Leach, J.S.L. (1988) The Anodic Oxidation of Valve Metals—II. The Influence of the Anodizing Conditions on the Transport Processes during the Anodic Oxidation of Zirconium. *Electrochimica Acta*, **33**, 1721-1727. https://doi.org/10.1016/0013-4686(88)85006-0

[26] Kuromoto, N.K., Simão, R.A. and Soares, G.A. (2007) Titanium Oxide Films Produced on Commercially Pure Titanium by Anodic Oxidation with Different Voltages. *Materials Characterization*, **58**, 114-121. https://doi.org/10.1016/j.matchar.2006.03.020

[27] Gudic, S., Radosevic, J. and Kliskic, M.K. (2002) Study of Passivation of Al and Al-Sn Alloys in Borate Buffer Solutions Using Electrochemical Impedance Spectroscopy. *Electrochimica Acta*, **47**, 3009-3016. https://doi.org/10.1016/s0013-4686(02)00246-3

[28] Orazem, M.E. and Tribollet, B. (2008) Electrochemical Impedance Spectroscopy. Wiley. https://doi.org/10.1002/9780470381588

[29] Wegrelius, L., Falkenberg, F. and Olefjord, I. (1999) Passivation of Stainless Steels in Hydrochloric Acid. *Journal of The Electrochemical Society*, **146**, 1397-1406. https://doi.org/10.1149/1.1391777

[30] Hamadou, L., Kadri, A. and Benbrahim, N. (2005) Characterisation of Passive Films Formed on Low Carbon Steel in Borate Buffer Solution (pH 9.2) by Electrochemical Impedance Spectroscopy. *Applied Surface Science*, **252**, 1510-1519. https://doi.org/10.1016/j.apsusc.2005.02.135

[31] Yanagisawa, K., Nakanishi, T., Hasegawa, Y. and Fushimi, K. (2015) Passivity of Dual-Phase Carbon Steel with Ferrite and Martensite Phases in Ph 8.4 Boric Acid-Borate Buffer Solution. *Journal of the Electrochemical Society*, **162**, C322-C326. https://doi.org/10.1149/2.0471507jes

[32] Alves, V.A. and Brett, C.M.A. (2002) Characterisation of Passive Films Formed on Mild Steels in Bicarbonate Solution by Eis. *Electrochimica Acta*, **47**, 2081-2091. https://doi.org/10.1016/s0013-4686(02)00077-4

[33] Etteyeb, N., Dhouibi, L., Takenouti, H., Alonso, M.C. and Triki, E. (2007) Corrosion Inhibition of Carbon Steel in Alkaline Chloride Media by Na_3PO_4. *Electrochimica Acta*, **52**, 7506-7512. https://doi.org/10.1016/j.electacta.2007.03.003

[34] Kim, Y.J. (2000) *In-Situ* Electrochemical Impedance Measurement of Oxide Film Formed on Type 304 Stainless Steel in High-Temperature Water. *Corrosion*, **56**, 389-394. https://doi.org/10.5006/1.3280542

[35] El-Taib Heakal, F., Ghoneim, A.A. and Fekry, A.M. (2007) Stability of Spontaneous Passive Films on High Strength Mo-Containing Stainless Steels in Aqueous Solutions. *Journal of Applied Electrochemistry*, **37**, 405-413. https://doi.org/10.1007/s10800-006-9271-3

[36] Scully, J.R. (2000) Polarization Resistance Method for Determination of Instantaneous Corrosion Rates. *Corrosion*, **56**, 199-218. https://doi.org/10.5006/1.3280536